Electronic Supplementary Material (ESI) for Journal of Materials Chemistry A.

Unraveling the amines oxidative coupling activity of hierarchical porous Fe–N_4–O_1 single–atom catalysts: Oxygen atoms-mediated dual reaction pathway

Hongwei He,[‡acd] Kui Ma,[‡b] Huibin Liu,[acd] Jing Li,[acd] Lirong Zheng,[e] Fengbao Zhang,[acd] Xiaobin Fan,[acd] Wenchao Peng,[acd] Junyi Ji*[b] and Yang Li*[acd]

[a] School of Chemical Engineering and Technology, Tianjin University, Tianjin 300354, P. R. China

[b] School of Chemical Engineering, Sichuan University, Chengdu 610065, P. R. China

[c] Haihe Laboratory of Sustainable Chemical Transformations, Tianjin 300192, P. R. China

[d] Institute of Shaoxing, Tianjin University, Zhejiang 312300, P. R. China

[e] Beijing Synchrotron Radiation Facility, Institute of High Energy Physics, Chinese Academy of Sciences, Beijing 100049, P. R. China

Supplementary experimental section

Sample characterization

The obtained hybrids were characterized by transmission electronic microscopy (TEM, JEM–2100 F) and scanning electron microscopy (SEM, Hitachi, S–4800), high–angle annular dark–field scanning transmission electron microscopy (HADDF–STEM), N_2 adsorption/desorption measurements (Bjbuilder, SSA–7000), X–ray photoelectron spectroscopy (XPS, Escalab 250 Xi), X–ray diffraction (XRD, AXS D8–Focus, Cu–Ka radiation). The reactions were monitored by ultraviolet–visible absorption spectroscopy (UV–DRS; Shimadzu UV–2600), gas chromatography (GC; Agilent 6890N GC–FID system) and electron paramagnetic resonance spectrometer (EPR, E580). X-ray absorption near-edge structure (XANES) and extended X-ray absorption fine structure (EXAFS) measurements were performed at 1W1B beamline of Beijing Synchrotron Radiation Facility (BSRF). The X-ray absorption spectra were detected in the transmission mode. Using the Athena program of the IFEFFIT package, the background of the spectra was removed by extrapolating the pre-edge region onto the EXAFS region, and the χ(E) data were normalized with respect to the edge jump step. Then the normalized χ(E) was transformed from energy space to k-space with χ(k) multiplied by k^3 to compensate for the contributions from light scatters. Finally, the $k^3\chi(k)$ data in k-space ranging from 3.0 to 10.0 $Å^{-1}$ were Fourier-transformed to R-space to get the radial structure function spectra (RSFs). The XANES spectra of Fe foil and Fe_2O_3 were employed as the references.

Methods for RSFs simulation

The χ(k) data of the processed EXAFS spectra were fitted in R space ranging from 1.0 to 2.0 Å with the Artemis program of the IFEFFIT package. From this simulation, structural parameters including coordination number (N), coordination distance (R), Debye-Waller factors (σ^2) and inner potential correction (ΔE_0) were obtained. Theoretical RSFs of the samples were calculated using FEFF and their crystal structure parameters searched in FindIt database were compiled as the input data.

DFT calculations

Vienna ab-initio simulation package (VASP) based on density functional theory (DFT) was used for the entire calculations.[1] Projector augmented wave (PAW) method and Perdew-Burke-Ernzerhof functional were adopted for describing the interactions of inner core and valence electrons and calculating the exchange and correlation energies [2, 3]. Cutoff energy was set to 400 eV, and Brillouin zone was conducted using a 1×1×1 Monkhorst-Pack grid. The structure was optimized until reaching convergence. The convergence precisions of energy and force were set to 1.0×10^{-5} and 0.02 eV/Å, respectively. Spin polarization and van der Waals force (DFT-D2) were considered for a higher accuracy.

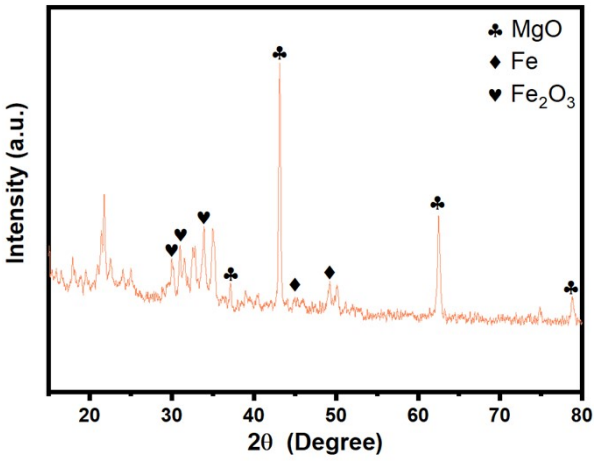

Fig. S1 The XRD pattern of Fe–NC before HCl treatment (wFe–NC). The diffraction peaks of metallic Fe (JCPDS number 50-1275), Fe_2O_3 (JCPDS number 40-1139) and MgO (JCPDS number 45-0946) are clearly observed in the XRD pattern.

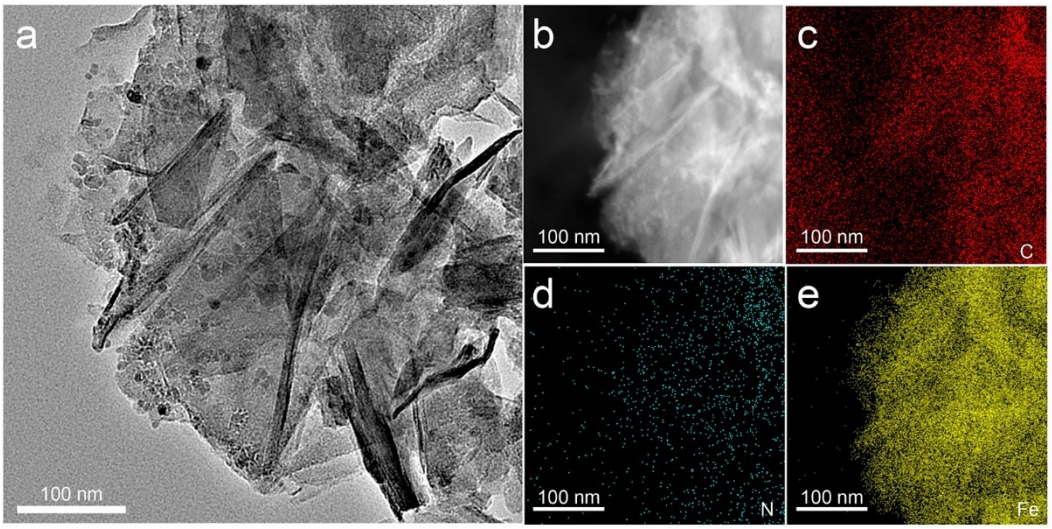

Fig. S2 The TEM (a), HADDF–STEM (b) and corresponding element maps showing the distribution of C (c), N (d) and Fe (e) images of wFe–NC.

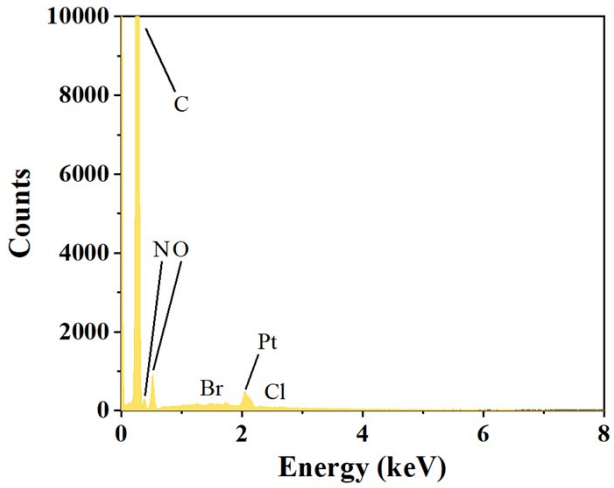

Fig. S3 EDS spectrum of Fe–NC. (The peak at 2.06 keV belongs to the platinum sprayed on the surface of the sample during the SEM test)

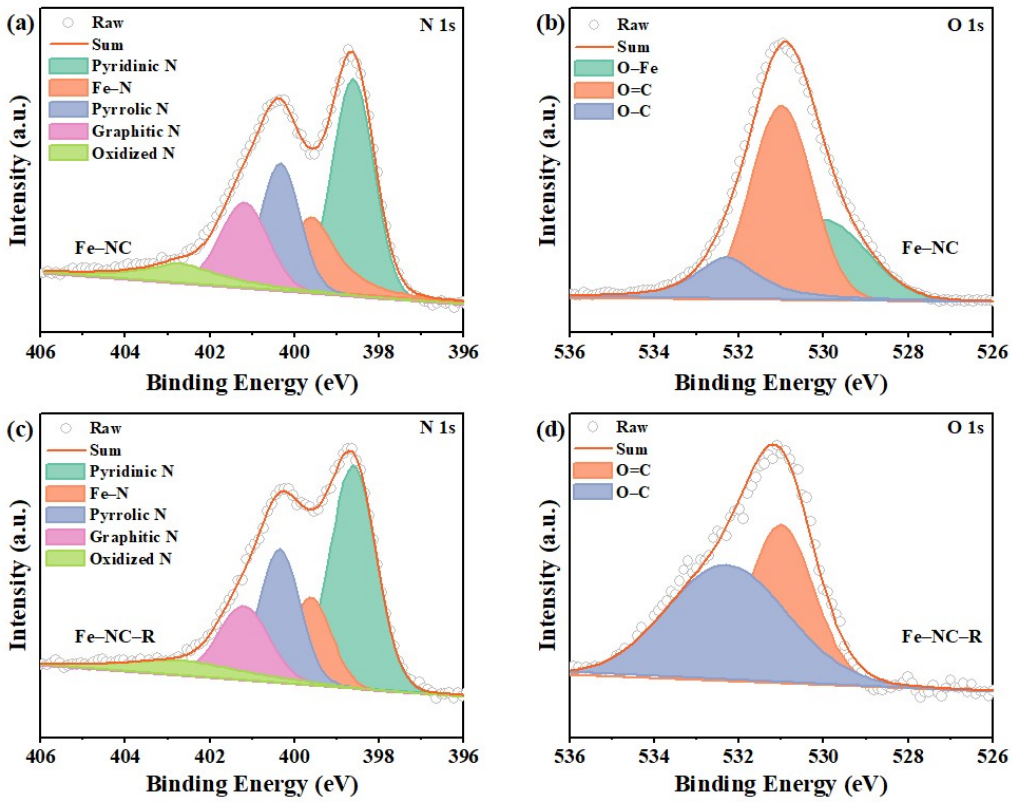

Fig. S4 The N 1s (a) and O 1s (b) high–resolution XPS spectrum of Fe–NC. The N 1s (c) and O 1s (d) high–resolution XPS spectrum of Fe–NC–R.

The N 1s high–resolution XPS spectrum of Fe–NC can be deconvoluted into pyridinic N (398.62 eV), Fe–N (399.6 eV), pyrrolic N (400.34 eV), graphitic N (401.2 eV) and oxidized N (402.7 eV), respectively (**Fig. S4a**). The O 1s high–resolution XPS spectrum of Fe–NC can be deconvoluted into O–Fe (530 eV), O=C (531 eV) and O–C (532.3 eV), respectively (**Fig. S4b**). Compared with the N 1s and O 1s high–resolution XPS spectra of Fe–NC, there is the peak of Fe–N in the N 1s high–resolution XPS spectrum of Fe–NC–R (**Fig. S4c**), but the peak of O–Fe is not observed in the O 1s high–resolution XPS spectrum of Fe–NC–R (**Fig. S4d**). These results further demonstrate that Fe–NC and Fe–NC–R possess FeN_4O_1 and FeN_4 configuration.

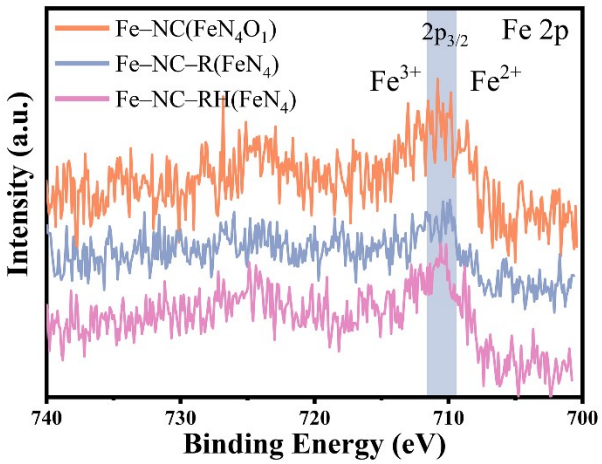

Fig. S5 XPS Fe 2p spectra of Fe–NC, Fe–NC–R and Fe–NC–RH, respectively.

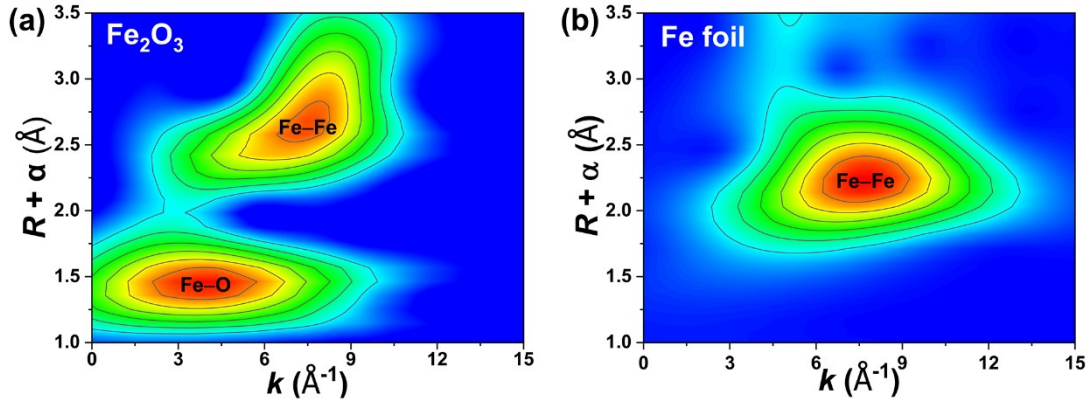

Fig. S6 Wavelet transform (WT) of the k^3-weighted EXAFS data of Fe_2O_3 (a) and Fe foil (b), respectively.

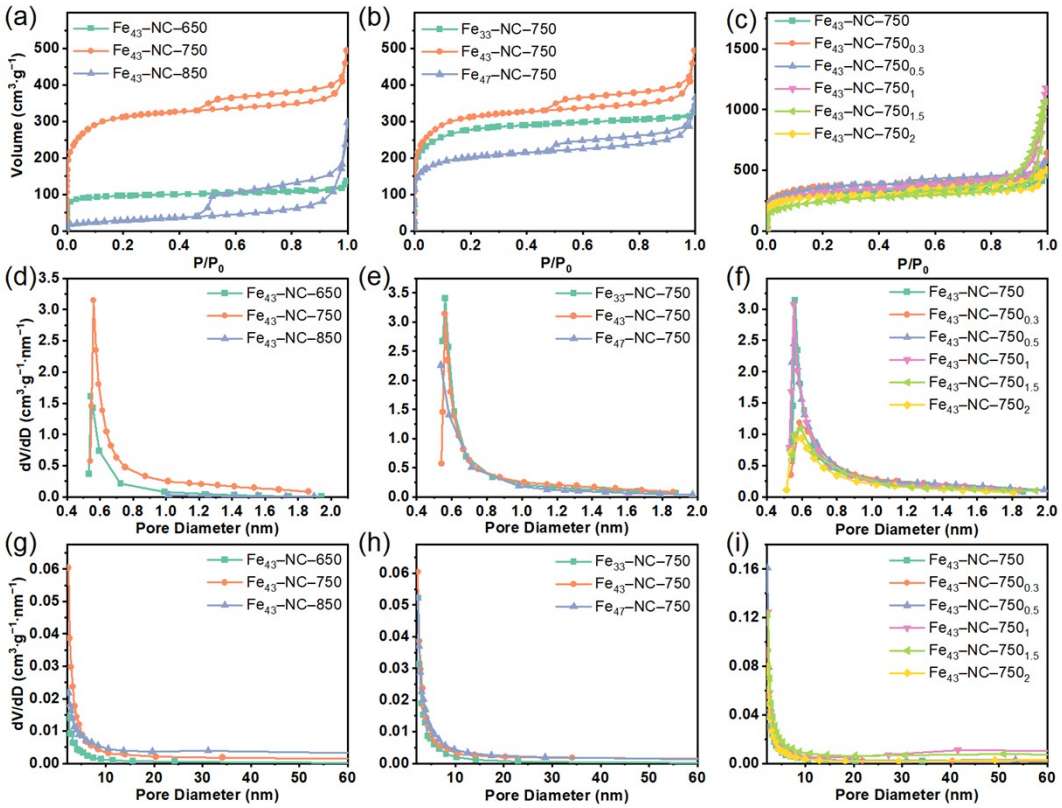

Fig. S7 Nitrogen adsorption-desorption isotherms of the catalysts with different pyrolysis temperature (a) and amounts of $FeCl_3$ (b) or MgO (c). as well as corresponding pore size distribution curves (d–i). All as–prepared catalysts are referred as Fe_x–NC–y_z (x represents the mass fraction of $FeCl_3$ in ionic liquid. y represents the pyrolysis temperature. z represents the amount of MgO.)

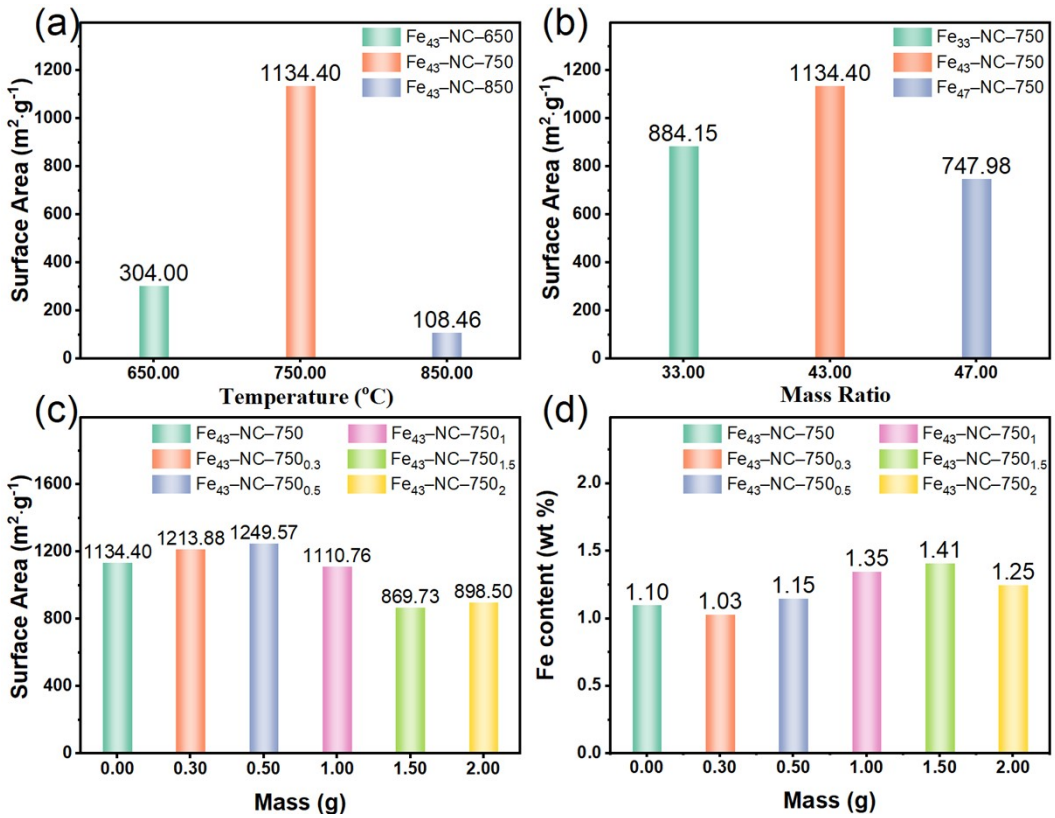

Fig. S8 The Brunauer–Emmett–Teller (BET) surface areas of catalysts with different pyrolysis temperature (a), contents of $FeCl_3$ in ionic liquid (b) and amounts of or MgO (c). (d) The Fe content in catalysts with different amounts of or MgO. All as–prepared catalysts are referred as Fe_x–NC–y_z (x represents the mass fraction of $FeCl_3$ in ionic liquid. y represents the pyrolysis temperature. z represents the amount of MgO.)

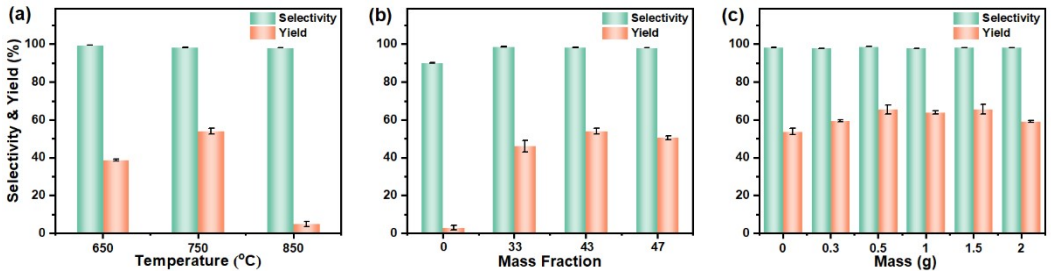

Fig. S9 The effect of the pyrolysis temperature (a), the content of $FeCl_3$ in ionic liquid (b) and the amount of MgO (c) on the catalytic performances of the catalysts[a)].

[a)]The reaction is carried out with benzylamine (2.5 mmol), catalyst (20 mg) and p-xylene (5 mL) at 120 °C for 4 h in air condition.

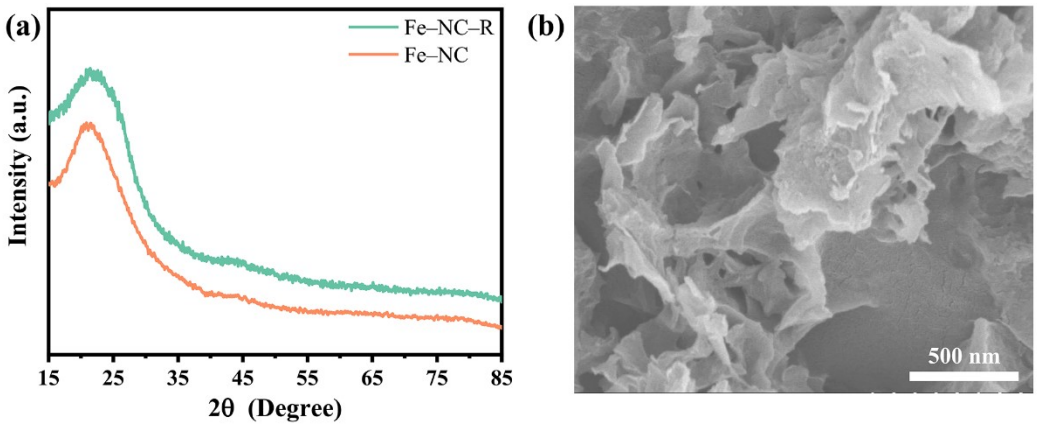

Fig. S10 (a) The XRD patterns of Fe–NC and Fe–NC–R. (b) The SEM image of Fe–NC–R.

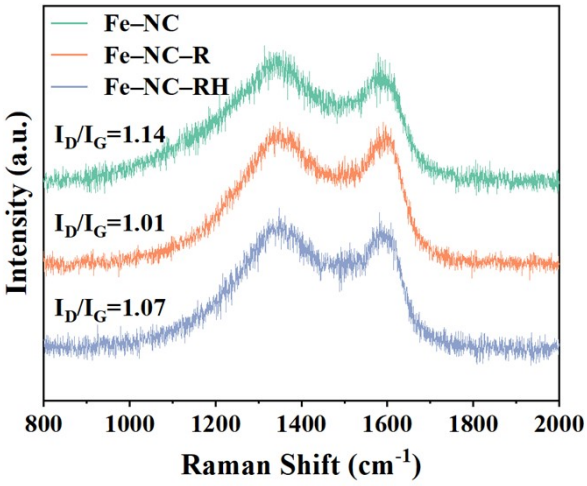

Fig. S11 Raman spectra of Fe–NC, Fe–NC–R and Fe–NC–RH.

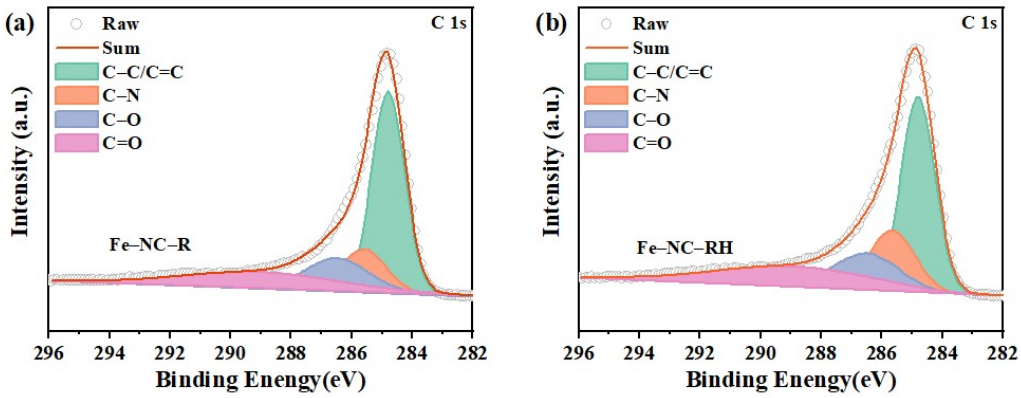

Fig. S12 The C 1s high–resolution XPS spectrum of Fe–NC–R (a) and Fe–NC–RH (b).

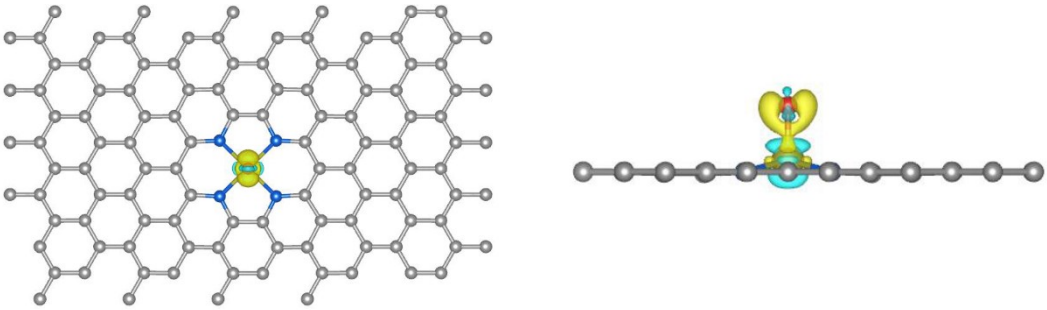

Fig. S13 Difference of charge density of Fe–NC(FeN_4O_1). (The isosurface level is 0.015 e$Å^{-3}$. The yellow and blue isosurface present electron donation and accumulation, respectively.)

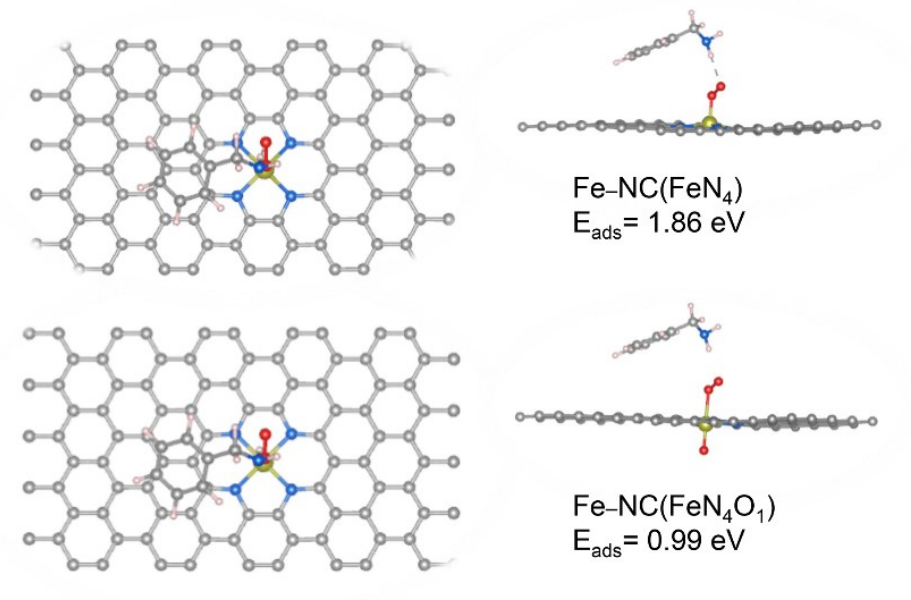

Fig. S14 Simulated structures of benzylamine and O_2 adsorbed on Fe–NC(FeN_4) and Fe–NC(FeN_4O_1), respectively.

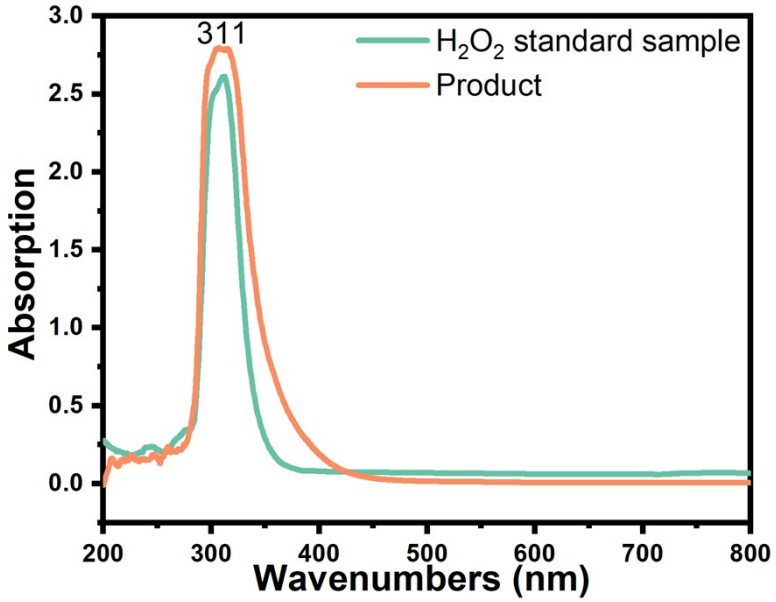

Fig. S15 Ultraviolet-visible absorption spectra the oxidation of benzylamine system.

Table S1. The Fe content in catalysts as determined by inductively coupled plasma mass spectrometry.

entry	catalyst	Fe content (wt %)
1	Fe_{43}–NC–750	1.1
2	Fe_{43}–NC–$750_{0.3}$	1.03
3	Fe_{43}–NC–$750_{0.5}$	1.15
4	Fe_{43}–NC–750_{1}	1.35
5	wFe–NC	30.11
6	Fe–NC	1.41
7	Fe–NC–R	1.5
8	Fe_{43}–NC–750_{2}	1.25

Table S2. The atomic percentages C, N, O and Fe in catalysts as determined by XPS.

entry	catalyst	C (at %)	N (at %)	O (at %)	Fe (at %)
1	Fe–NC	64.56	13.93	21.16	0.35
2	Fe–NC–R	79.87	14.53	5.32	0.27
3	Fe–NC–RH	79.65	15.17	4.80	0.38

Table S3. Structural parameters extracted from the Fe K-edge EXAFS fitting. (S_0^2 = 0.817)

Sample	Scattering pair	CN	R(Å)	σ^2	ΔE_0(eV)	R factor
Fe foil	Fe–Fe(1)	8*	2.46	0.0059	5.52	0.007
	Fe–Fe(2)	6*	2.84	0.0058	5.52	0.007
Fe–NC	Fe–O	1.37	2.07	0.0002	1.05	0.015
	Fe–N	3.75	1.98	0.0002	1.05	0.015
Fe–NC–R	Fe–N	1.99	1.95	0.0009	0.074	0.019
	Fe–N	1.99	1.93	0.0009	0.074	0.019

S_0^2 is the amplitude reduction factor, obtained by fitting the standard sample; CN is the coordination number; R is interatomic distance (the bond length between Fe central atoms and surrounding coordination atoms); σ^2 is Debye–Waller factor (thermal and static disorder in absorber-scatterer distances); ΔE_0 is edge–energy shift. R factor is used to assessment the goodness of the fitting.

* Represents the value was fixed during EXAFS fitting, based on the known structure of Fe metal.

Table S4. The atomic percentages of surface functional groups from deconvoluted C 1s XPS spectral fitting.

Catalyst	C–C/C=C	C–N	C–O	C=O
Fe–NC–R	49.63%	14.39%	16.06%	19.92%
Fe–NC–RH	46.64%	18.79%	15.50%	19.07%

Table S5. Comparison of TOF with Fe–NC and other reported catalysts for the oxidative coupling reaction of benzylamine.

catalyst	TOF (h^{-1})	Ref.
V–N–V–600	53.9 [a]	4
Meso Cs/MnOx	1.11 [b]	5
GCN–(Cu)	14 [c]	6
$Cu_{meth}Al_{butox}$	<0.5 [d]	7
Fe–NC	58.91 [e]	This work

[a]TOF was calculated as moles of benzylamine converted per mole of V sites and a reaction time of 2 h. [b]TOF was calculated as moles of benzylamine converted per mole of catalyst and a reaction time of 3 h. [c]TOF was calculated as moles of benzylamine converted per mole of Cu sites and a reaction time of 24 h. [d]TOF was calculated as moles of benzylamine converted per mole of catalyst and a reaction time of 20 h. [e]TOF was calculated as moles of benzylamine converted per mole of Fe sites and a reaction time of 4 h.

References

1. G. Kresse and J. Furthmüller, *Phys. Rev. B*, 1996, **54**, 11169.
2. P. E. Blöchl, *Phys. Rev. B*, 1994, **50**, 17953-17979.
3. J. P. Perdew, K. Burke and M. Ernzerhof, *Phys. Rev. Lett.*, 1996, **77**, 3865.
4. Q. Xu, B. Feng, C. Ye, Y. Fu, D. Chen, F. Zhang, J. Zhang and W. Zhu, *ACS Appl. Mater. Interfaces*, 2021, **13**, 15168-15177.
5. S. Biswas, B. Dutta, K. Mullick, C. H. Kuo, A. S. Poyraz and S. L. Suib, *ACS Catal.*, 2015, **5**, 4394-4403.
6. A. Bakandritsos, R. G. Kadam, P. Kumar, G. Zoppellaro, M. Medved, J. Tucek, T. Montini, O. Tomanec, P. Andryskova, B. Drahos, R. S. Varma, M. Otyepka, M. B. Gawande, P. Fornasiero and R. Zboril, *Adv. Mater.*, 2019, **31**, e1900323.
7. D. Dissanayake, L. A. Achola, P. Kerns, D. Rathnayake, J. He, J. Macharia and S. L. Suib, *Appl. Catal., B*, 2019, **249**, 32-41.